PHYSICAL REVIEW B **89**, 195105 (2014)

Unconventional quantum criticality in the kicked rotor

Jiao Wang,[1] Chushun Tian,[2] and Alexander Altland[3]
[1]*Department of Physics and Institute of Theoretical Physics and Astrophysics, Xiamen University, Xiamen 361005, China*
[2]*Institute for Advanced Study, Tsinghua University, Beijing 100084, China*
[3]*Institut für Theoretische Physik, Universität zu Köln, Köln 50937, Germany*

(Received 3 February 2014; revised manuscript received 22 April 2014; published 7 May 2014)

The quantum kicked rotor (QKR) driven by d incommensurate frequencies realizes the universality class of d-dimensional disordered metals. For $d > 3$, the system exhibits an Anderson metal-insulator transition which has been observed within the framework of an atom-optics realization. However, the absence of genuine randomness in the QKR reflects in critical phenomena beyond those of the Anderson universality class. Specifically, the system shows strong sensitivity to the algebraic properties of its effective Planck constant $\tilde{h} \equiv 4\pi/q$. For integer q, the system may be in a globally integrable state, in a "supermetallic" configuration characterized by diverging response coefficients, Anderson localized, metallic, or exhibit transitions between these phases. We present numerical data for different q values and effective dimensionalities, with the focus on parameter configurations which may be accessible to experimental investigations.

DOI: 10.1103/PhysRevB.89.195105 PACS number(s): 05.45.Mt, 64.70.Tg, 72.15.Rn, 71.30.+h

I. INTRODUCTION

The (quasiperiodic) quantum kicked rotor is a quantum particle on a unit radius ring whose dynamics is described by the time-dependent Hamiltonian

$$\hat{H}(t) = \frac{1}{2}(\tilde{h}\hat{n})^2 + K\cos\hat{\theta}\, f_d(t) \sum_m \delta(t-m), \qquad (1)$$

where $\hat{\theta}$ and $\hat{n} = -i\partial_\theta$ are coordinate and angular momentum operator, respectively. The Hamiltonian $\hat{H}$ describes kicking of the particle at unit time intervals with an amplitude depending on the angular position. The quasiperiodic quantum kicked rotor given by Eq. (1) differs from its more widely known sibling, the standard quantum kicked rotor (QKR) ($d = 1$) [1], in that the kicking strength itself $\sim K f_d(t)$ is explicitly time dependent, where the modulating function $f_d(t) = \prod_{i=1}^{d-1} \cos(\omega_i t + \phi_i)$ depends on $d-1$ incommensurate frequencies ω_i. (ϕ_i are constant phase offsets.) Much like the fact that the standard QKR has been shown to lie in the universality class of quasi-one-dimensional disordered metals [2–7], the quasiperiodic QKR corresponds to a d-dimensional metal [8]. (The mapping to a d-dimensional effective system will be made explicit below.) The Anderson localization phenomena characteristic for both one-dimensional [9] and higher-dimensional [10–12] metallic systems have been seen in cold-atom experiments. Strikingly, a three-dimensional quasiperiodic QKR has been experimentally shown to undergo an Anderson metal-insulator transition upon variation of the kicking amplitude.

The fact that the rotor is a deterministic chaotic rather than a stochastic disordered system manifests itself in various anomalies emerging at specific values of the global kicking strength K and Planck's constant $\tilde{h}$. Of particular interest are values $\tilde{h}/(4\pi) = p/q$, where p,q are coprime integers. At these "resonant" values, the Hamiltonian (1) commutes with translations $\hat{n} \to \hat{n} + q$ in angular momentum space, and the $d = 1$ rotor effectively behaves like a ring in angular momentum space of circumference q. If q is smaller than the localization length ξ, it ceases to be localized, and an observable consequence of this phenomenon is a quadratic growth of the rotor's energy at large times; see Refs. [2,7,13,14] for review. (For the exceptional case ($p = 1, q = 2$) of the "quantum antiresonance," cf. Refs. [2,15,16].) For q larger than ξ, the quantum resonance reduces to an exponentially small [in $\exp(-q/\xi)$] correction to a localized background, and it vanishes as irrational values of $\tilde{h}/(4\pi)$ are approached.

In Refs. [8,17], we have analytically shown that in $d > 1$, the same mechanism may lead to a type of quantum criticality, outside the Anderson universality class. Basic features of this phenomenon can be understood by observing that at the resonant values, the rotor becomes effectively finite in the n coordinate, while it remains infinitely extended in the $d-1$ auxiliary dimensions associated to the additional driving frequencies [8]. Upon compactification of the "unit cell" in the n direction, the system assumes the topology of a d-dimensional cylinder (cf. Fig. 1), and physical observables such as the expectation value of the rotor's energy, $E(t) \equiv \langle \hat{n}(t)^2 \rangle$, can be computed by probing its sensitivity to changes in the boundary conditions in the compact n direction.

Equivalently, we may characterize the system's behavior in terms of the Fourier transform, $E(t) = -\int \frac{d\omega}{2\pi}\frac{e^{-i\omega t}}{\omega^2}\sigma(\omega)$, where $\sigma(\omega)$ plays a role analogous to the optical conductivity of a metal [7,8]. Specifically, the difference between a linear and a quadratic temporal increase of $E(t)$ manifests itself in the optical conductivity as

$$\sigma(\omega) \xrightarrow{\omega\to 0} \begin{cases} \text{vanishing}, & \text{insulator} \\ \text{finite constant}, & \text{metal} \\ 1/(-i\omega), & \text{supermetal}. \end{cases} \qquad (2)$$

(In solid-state physics, a $\sim \omega^{-1}$ divergent optical conductivity would be observed, e.g., for the perfect resonant transport through a clean quantum dot with a discrete spectrum—hence the terminology "supermetal." Within the present context, the divergence is a manifestation of the discreteness of the spectrum in a system localized in the auxiliary dimensions, but finite in the physical direction [7,8]).

A saturation of the energy in large times reflects in the vanishing of the low-frequency conductivity—the insulator. Whether the system displays metallic or supermetallic

©2014 American Physical Society

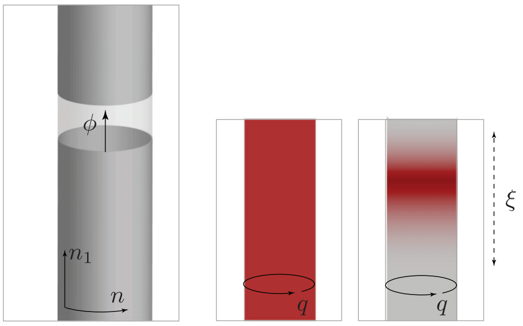

(a) (b)

FIG. 1. (Color online) Angular momentum space of the quasiperiodic QKR at a resonant value $\tilde{h} = 4\pi p/q$. The system becomes effectively finite in the n direction, but remains infinite in its $d-1$ auxiliary dimensions ($d=2$ in the figure.) Physical observables can be computed by probing the sensitivity to boundary conditions in the n direction or, equivalently, to a Bloch phase, $\phi \in [0,2\pi/q]$, which may be interpreted as an Aharonov-Bohm flux piercing the system. The ensuing physics then crucially depends on whether wave functions are a) extended or b) localized in the auxiliary directions.

behavior crucially depends on the localization properties in the infinitely extended $d-1$ dimensions of the cylinder (cf. Fig. 1.) In dimensions $d>3$, above the Anderson metal-insulator transition, wave functions are extended in the $d-1$ auxiliary dimensions; the system then resembles an (ordinary) metal, with finite (zero-frequency) optical conductivity manifesting itself in a linear energy growth in large times. However, below the Anderson transition, or in low dimensions $d \leqslant 3$, wave functions are localized in the $d-1$ auxiliary dimensions, which means that "transport" in the n direction is via a discrete spectrum of (localized) states. In this phase, the system has much in common with a supermetallic quantum dot and the discreteness of its spectrum implies a diverging optical conductivity manifesting in a quadratic energy growth in large times. Somewhat counterintuitively, this supermetallic conduction behavior is rooted in strong Anderson localization in the transverse directions. As such, a supermetal simulates a perfect one-dimensional crystal of lattice constant q, with complex unit cell structures of finite spatial extension in other $d-1$ dimensions.

In Ref. [8], the existence of a supermetallic phase in low dimensions, and of a metal-supermetal transition in dimensions $d>3$, was predicted on the basis of a field theoretic analysis. The purpose of the present paper is to put these results to a numerical test. We will also pay attention to anomalies arising at small values $q=1,2$ where the system is integrable (nonchaotic) and, at the same time, exactly solvable. For these values, quasiperiodic oscillatory patterns rather than localization are observed (cf. the left column of Table I in which the main observations of this paper are summarized). We have also found anomalies at $q=4$, where the motion is partially regular, the generic picture breaks down, and metallic regimes are absent (Table I, right column.) The general conclusion will be that the adjustability of the two principal parameters $(K,\tilde{h})$ provides us with a spectrum of opportunities to realize critical phenomena pertaining to the physics of regular versus chaotic dynamics, and localization. The physics addressed in the present paper should be well in reach of current experiments [10–12].

The rest of the paper is organized as follows: in Sec. II, we introduce the Floquet operator underlying our analysis. In Secs. III–V, we simulate its dynamics to explore the behavior at the smallest resonant values $q=1,2$, "generic" resonant values $q=3,5,\ldots$, and the anomalous value $q=4$, respectively. We conclude in Sec. VI, and a number of technical details are presented in the Appendix A. The physics discussed in this work is insensitive to the value of p and we set $p=1$ throughout.

II. FLOQUET OPERATOR

Below, we will apply fast Fourier transform techniques to simulate the quantum evolution of the initial state $|n \equiv 0\rangle$ at integer times t as

$$|\psi(t)\rangle = \prod_{s=1}^{t} \hat{U}'(s)|0\rangle, \tag{3}$$

$$\hat{U}'(s) \equiv e^{-\frac{i\tilde{h}\hat{n}^2}{2}} e^{-\frac{iK}{\tilde{h}} f_d(s)\cos\hat{\theta}}. \tag{4}$$

Using these states, we numerically compute the expectation value $E'(t) = \langle \hat{n}^2(t)\rangle = -\langle\psi(t)|\partial_\theta^2|\psi(t)\rangle$ to learn about the physical properties of the system. The operator (4) explicitly depends on the discrete time s, and in this nonautonomicity hides the effective dimensionality of the system. Following ideas introduced in Refs. [8,18], we briefly review how the time dependence of $\hat{U}'$ may be eliminated at the expense of introducing $d-1$ additional dimensions. To this end, let us interpret $|\theta_0 \equiv \theta,\theta_1,\ldots,\theta_{d-1}\rangle$ as a d-dimensional coordinate vector, comprising a "real" angular coordinate θ and a generalization of the parameters $\theta_{i\geqslant 1}$ entering the definition of the kicking function f_d to "virtual" coordinates. Corresponding to the "coordinate state," we have a d-dimensional angular momentum state, $|n_0 \equiv n,n_1,\ldots,n_{d-1}\rangle$, where $\hat{n}_i \equiv -i\partial_{\theta_i}$ is

TABLE I. Summary of main results.

	$q=1,2$		$q=3,5,6,\ldots$			$q=4$		
Parameter	$\langle\hat{n}^2(t)\rangle$	Phase	$\langle\hat{n}^2(t)\rangle$	Phase	Crossover time	$\langle\hat{n}^2(t)\rangle$	Phase	Crossover time
$d=2$	Quasiperiodic oscillation	Insulator (non-Anderson)	$\sim t^2$	Supermetal	$t_\xi \sim K^2$	$\sim t^2$	Supermetal	$t_\xi \sim K$
$d=3$					$\ln t_\xi \sim K^2$			
$d=4$			$\sim t^2$ $(K<K_c)$	Supermetal	$t_\xi \sim (K_c-K)^{-\alpha}$			
			$\sim t$ $(K \geqslant K_c)$	Metal	∞			

conjugate to θ_i. The gauge transformed operator,

$$\hat{U} \equiv e^{-i(s+1)\sum_{i=1}^{d-1}\omega_i\hat{n}_i}\hat{U}'(s)e^{is\sum_{i=1}^{d-1}\omega_i\hat{n}_i}$$
$$= e^{-i(\frac{\tilde{h}\hat{n}^2}{2}+\sum_{i=1}^{d-1}\omega_i\hat{n}_i)}e^{-\frac{iK}{\tilde{h}}\prod_{i=0}^{d-1}\cos\hat{\theta}_i}, \quad (5)$$

then turns out to be time independent. This is the Floquet operator acting in the effectively d-dimensional Hilbert space corresponding to the states above.

Physical observables are to be computed at a fixed value of the phases $(\theta_1,\ldots,\theta_{d-1})$, which means a trace over the conjugate momenta. In the definition of our observables $E(t)$, this trace is implicit. In the following sections, we will explore the behavior of the expectation value for various values of the parameters q,K,d. In doing so, we will be met with different types of behavior, where a saturation $E(t) \xrightarrow{t\to\infty}$ const indicates Anderson localization, $E(t) \sim t$ is a characteristic for diffusive dynamics in the angular momentum space, and $E(t) \sim t^2$ is a characteristic for supermetallic behavior. In cases with localization, the time $t \sim t_\xi$ at which saturation sets in marks the localization time. Finally, persistent quasiperiodic fluctuations in $E(t)$ are indicative of integrable dynamics.

In our simulations below, we will employ both representations, $\hat{U}$ and $\hat{U}'$, and the expectation values $\langle\hat{n}^2(t)\rangle$ obtained in this way will be denoted $E(t)$ and $E'(t)$, respectively. The gauge equivalence of the two representations implies $E(t) = E'(t)$.

III. QUASIPERIODIC OSCILLATION AT $q = 1,2$

For $q = 1,2$, it is straightforward to verify (see Appendix A for details of the derivation) that

$$\frac{\langle\hat{n}^2(t)\rangle}{\frac{1}{2}(K/\tilde{h})^2} = \begin{cases} \left[\sum_{s=1}^{t} f_d(s)\right]^2, & q = 1 \\ \left[\sum_{s=1}^{t}(-)^s f_d(s)\right]^2, & q = 2. \end{cases} \quad (6)$$

This shows that $E(t)/[\frac{1}{2}(K/\tilde{h})^2]$ collapses onto a universal curve, independent of K but dependent on d. Figure 2 compares simulations and the analytical result (6) for $d = 3$, $q = 2$, and parameters $(\omega_1,\phi_1) = 2\pi[(\sqrt{5}-1)/2,\sqrt{3}-1]$, $(\omega_2,\phi_2) = 2\pi(\sqrt{2},\sqrt{11}-3)$. Analytical results and numerics are in perfect agreement. The curves illustrate how the rotor's energy exhibits quasiperiodic oscillations of rather small amplitude. The immobility of the system in n space effectively makes it a (non-Anderson) insulator. In the Appendix A, we calculate the right-hand side of Eq. (6) analytically to explicitly show that $E(t)$ exhibits quasiperiodic oscillations for $d = 2$. The existence of quasiperiodic oscillations in $E(t)$ for $q = 1,2$ is independent of the values of K and of $d \geqslant 2$. It reflects the regular nature of quantum dynamics.

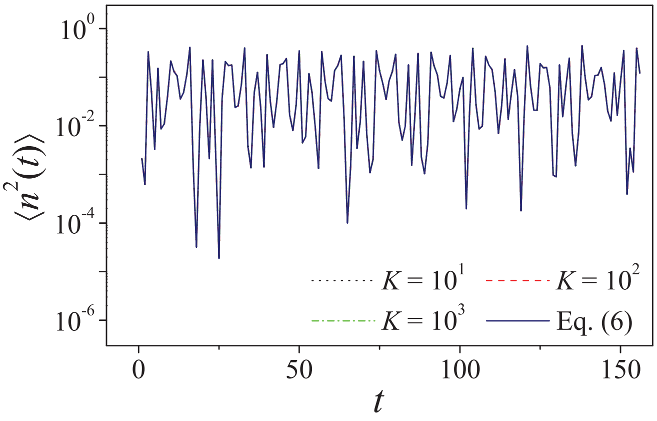

FIG. 2. (Color online) Both simulations and analytic results—in perfect agreement—show that $\langle\hat{n}^2(t)\rangle$ [in units of $\frac{1}{2}(K/\tilde{h})^2$] exhibits quasiperiodic oscillations.

Equation (6) also holds for the $d = 1$ standard rotor. Upon substitution of $f_1(s) \equiv 1$, it reproduces the well-known results [2,15], i.e., $E(t) \sim t^2$ for $q = 1$ and $E(t) \sim \delta_{P_t,-1}$ for $q = 2$, where P_t is the parity of the (discrete) time t: $P_t = +1$ (-1) for even (odd) t. (Recall the initial state $|n \equiv 0\rangle$.) The former describes an unbounded quadratic energy growth which is a characteristic of quantum resonance, while the latter describes a bounded time-periodic oscillation of energy (with a period of 2) which is a characteristic of quantum antiresonance. Interestingly, although behaviors of standard and quasiperiodic kicked rotors at $q = 1,2$ are fundamentally different, they are "unified" by the simple analytic formula (6).

IV. METAL-SUPERMETAL TRANSITION AT $q = 3,5,6,\ldots$

We now consider the value $q = 3$, which defines the first configuration where integrability is lost. The resulting phenomenology crucially depends on the effective dimensionality of the system, and we discuss various cases separately. Numerically, we have found the system's behavior at $q = 5,6,7,\ldots$ is the same as at $q = 3$.

A. QKR as a supermetal at $d = 2,3$

To realize a d-dimensional system, we modulate the pulse amplitude with one frequency ω_1 $(d = 2)$ and simulate the dynamics (4) with the parameters (ω_1,ϕ_1) given above. Results for $E(t)$ are shown in Fig. 3(a), where the $\sim t^2$ asymptotic at large times reflects supermetallic behavior. For large K (e.g., $K = 64$), the energy growth displays a clear metal-supermetal crossover.

To better expose its origin, we simulate the two-dimensional dynamics in terms of $\hat{U}$, given by Eq. (5), and compare the expectation value $E(t) = \langle\hat{n}^2(t)\rangle$ to the momentum dispersion in the virtual direction $\langle\hat{n}_1^2(t)\rangle$. The results shown in Fig. 3(b) demonstrate localization in the virtual n_1 direction and delocalization in the real n direction. It is also evident that the crossover to supermetallic growth and localization in the virtual direction take place at the same time, $t_\xi(K)$. The inset of Fig. 3(b) explicitly shows the exponential decay of a wave-function amplitude projected onto the n_1 direction, denoted as $P(n_1)$. These results indicate that the analytic predictions obtained for large q in Refs. [8,17] remain valid even for small q.

We next discuss the scaling behavior of $t_\xi(K)$. To this end, we extrapolate the short- and the long-time power laws pertaining to the metallic (supermetallic) growth to larger (smaller) times in $E'(t)$. In a double-logarithmic representation, this produces two straight lines with a crossing point whose time coordinate we identify with t_ξ [cf. Fig. 3(a)]. The results of this analysis are shown in Fig. 4(a), and a power-law fit obtains $t_\xi \propto K^{1.95\pm0.05}$. This is in excellent agreement with

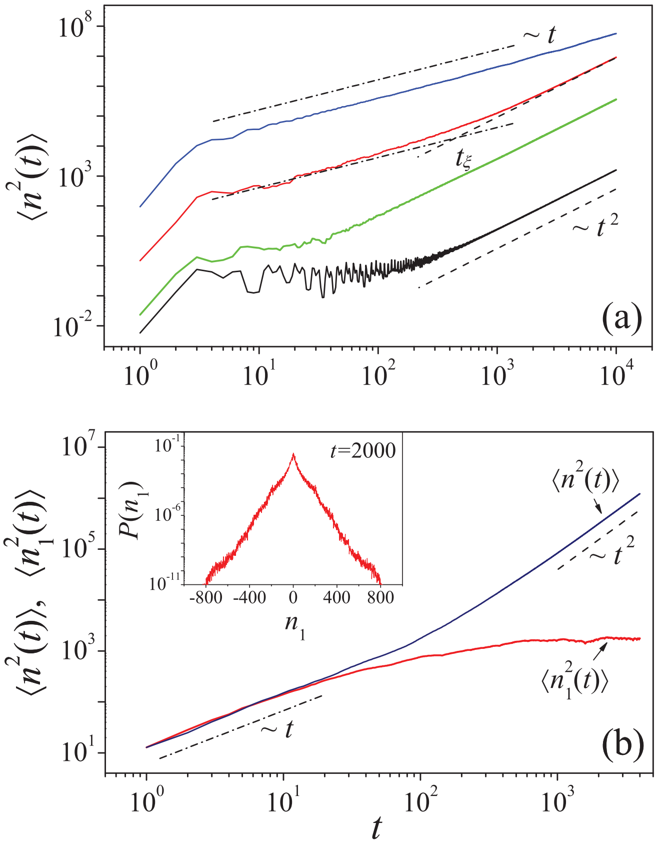

FIG. 3. (Color online) (a) For $d = 2$,$q = 3$, the QKR exhibits a supermetallic energy growth, $\langle \hat{n}^2(t)\rangle \sim t^2$, at large times. From bottom to top, the solid curves are for $K = 4$, 8, 64, and 512, respectively. (b) The saturation of $\langle \hat{n}_1^2(t)\rangle$ and the supermetallic growth of $\langle \hat{n}^2(t)\rangle$ simultaneously occur. $K = 30$. Inset: quasi-one-dimensional Anderson localization in the n_1 direction.

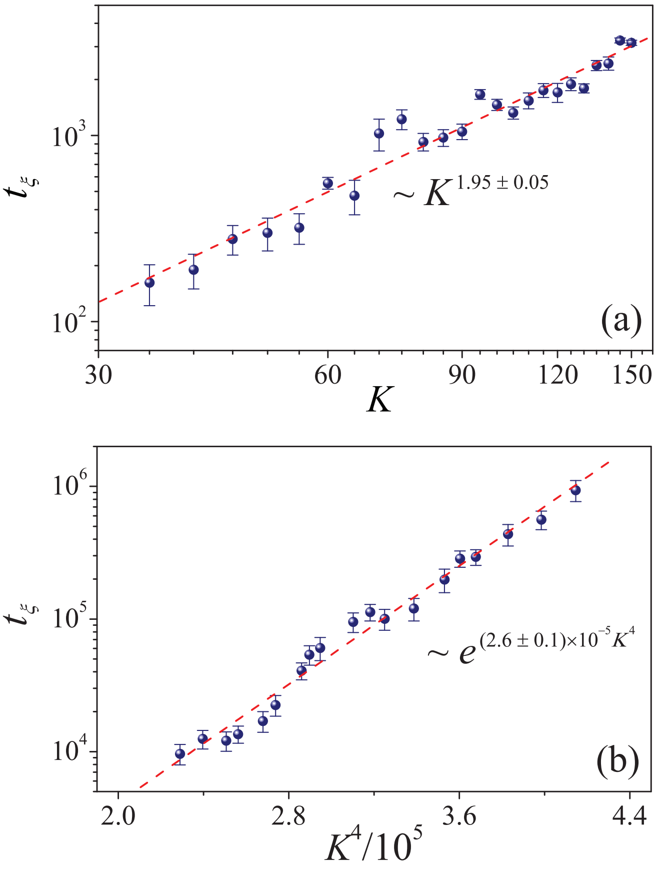

FIG. 4. (Color online) The scaling behavior of t_ξ for (a) $d = 2$ and (b) $d = 3$ at $q = 3$ in the system (4). The dashed lines are for the best linear fitting results.

the analytic prediction [8,17] $t_\xi \propto D \overset{q,K\gg1}{\sim} K^2$, where D is the classical diffusion coefficient. At small values of K, the diffusion constant becomes subject to short-time correlation corrections oscillatory in K, and this leads to the growth of deviations off the K^2 asymptotic.

The above results show that the behavior of $E(t)$ at $q = 3$ is explained by the same physical mechanisms as in the analytically studied $q \gg 1$ case: for short times, $t \ll t_\xi$, the dynamics of wave packets in angular momentum space is diffusive. At the corresponding frequency scales, $\omega \sim t^{-1} \gg t_\xi^{-1} \sim \Delta_\xi$, where Δ_ξ is the spacing between adjacent localized levels, the spectrum probed by the response function effectively looks continuous, or metallic. In the long-time regime, $t \gg t_\xi$, wave packets are localized, and the conjugate frequencies $\omega \ll \Delta_\xi$ are small enough to probe individual localized states. A straightforward analysis [8,17] shows that this leads to a divergent optical conductivity or quadratic scaling $\sim t^2$ of the function $E(t)$.

In the case of $d = 3$, simulations of the rotor driven by two frequencies $\omega_{1,2}$ show that $E'(t)$ crosses over from linear to quadratic increase at time $\sim t_\xi$, as in $d = 2$. However, as shown in Fig. 4(b), t_ξ now grows exponentially in $K^4 \sim D^2$. Again we see that at small values of K, short-time correlation corrections oscillatory in K lead to the growth of deviations off the K^4 asymptotic. This scaling reflects the exponential dependence of the localization length on the square of the diffusion coefficient characteristic for effectively two-dimensional [localization is in the $(d-1)$-dimensional virtual space] disordered systems [8]. This is a manifestation of unitary Anderson localization in the two-dimensional virtual space, as expected by the field theoretic analysis [7,8,17].

Indeed, the q periodicity in the n direction introduces an Aharonov-Bohm flux ϕ, namely, the Bloch momentum piercing the system (cf. Fig. 1), which effectively breaks the time-reversal symmetry of quantum dynamics within a unit cell. To confirm this symmetry, we further perform a study of spectrum statistics. To this end, we approximate $\omega_{1,2}/(2\pi)$ by rational number and compactify the unit cell in the $n_{1,2}$ direction. For the ensuing torus, we perform numerical diagonalization and find the quasienergy spectrum for fixed Bloch momentum ϕ. Then, by scanning ϕ, we obtain a large ensemble. This allows us to compute the level spacing distribution, denoted as $P(s)$. As exemplified in Fig. 5(a), the results are in excellent agreement with the Wigner surmise for the circular unitary ensemble (CUE). (We recall for the standard one-dimensional QKR, it has been analytically shown that the unitary symmetry leads to a simple, universal linear to quadratic crossover in the rotor's energy growth [7]).

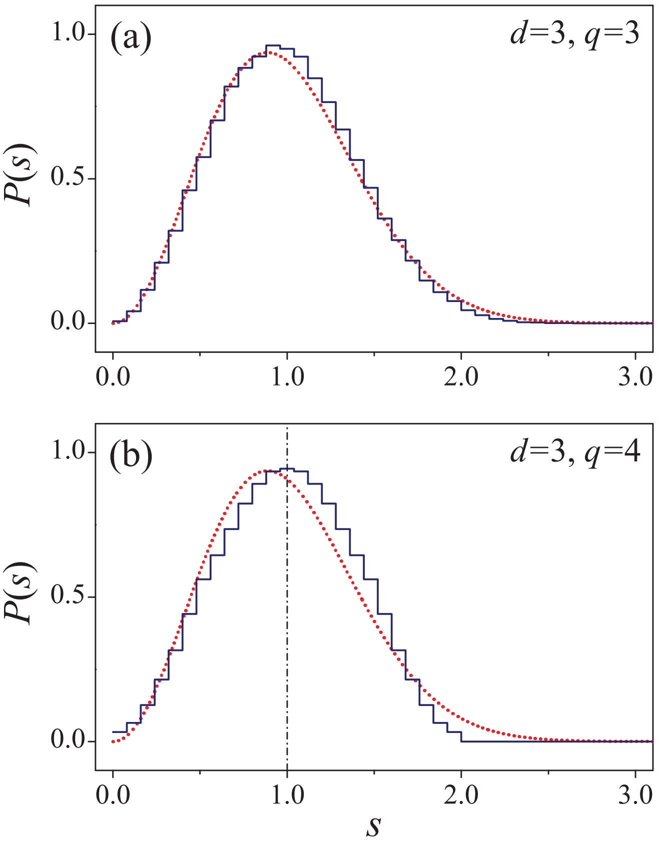

FIG. 5. (Color online) The level spacing distribution (histogram) for (a) $q = 3$ and (b) $q = 4$ in the three-dimensional system (5) with $K = 80$. The red dotted lines in both panels represent the Wigner surmise for CUE. Note that in (b), $P(s)$ is symmetric with respect to $s = 1$. The parameters $\omega_{1,2}/(2\pi)$ are approximated by 13/21 and 23/17, respectively.

B. Metal-supermetal transition at $d = 4$

Moving up in dimensionality, we introduce a third frequency/phase pair $(\omega_3,\phi_3) = 2\pi[(\sqrt{7}+1)/2, \sqrt{17}-4]$ to simulate the system at $d = 4$. Figure 6 shows results of $E(t)$ for different values of K. Our simulations indicate that at $K_c = 11.8 \pm 0.1$, the long-time behavior undergoes a transition from quadratic to linear large-time asymptotics. This is the Anderson transition separating an Anderson localized from a metallic phase in three-dimensional virtual space. We have found that the localization time for small deviations of K off the critical values scales as $t_\xi \sim (K_c - K)^{-\alpha}$ (Fig. 6 inset) with a critical exponent $\alpha = 4.5 \pm 0.3$. These observations are again in agreement with the large-q results obtained in Ref. [8].

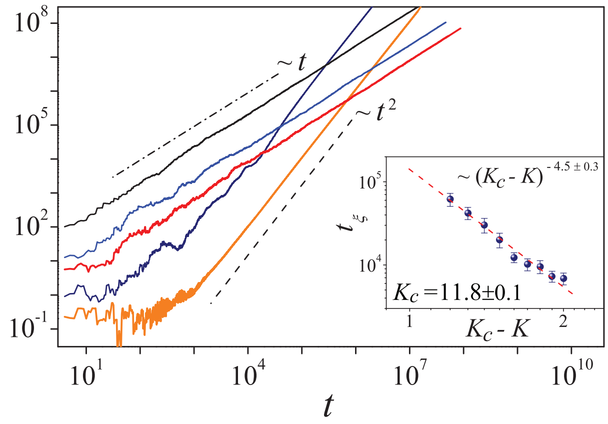

FIG. 6. (Color online) For $d = 4$ and $q = 3$, the QKR displays a metal-supermetal transition as K decreases. From bottom to top, at the left side, the solid curves are for $K = 4,8,20,30$, and 80, respectively. Inset: The crossover time t_ξ exhibits criticality.

Unlike in $d = 2,3$, simulations of the four-dimensional operator (5), i.e., of the function $E(t)$, are difficult. However, the observed value of K_c and the value of the critical exponent α can both be understood from scaling arguments: Anderson localization in virtual space leads to a frequency-dependent renormalization of the diffusion coefficient, $D \to D(\omega)$, where ω is Fourier conjugate to the observation time. Similar to discussions in Sec. IV A, the periodicity in the n direction renders Anderson transition in the $(d-1)$-dimensional virtual space of a unitary type. Correspondingly, by using the standard renormalization-group analysis, the leading (localization) correction is given by $D(\omega) \approx D[1 - \frac{1}{2\pi q^2 D}\int \frac{d^{d-1}\phi}{(2\pi)^{d-1}}(-i\omega + D\phi^2)^{-1}]$. For $d \geqslant 3$, the integral suffers ultraviolet divergence and requires a short-distance cutoff $\sim O(K/\tilde{h})$. Then, a rough estimate for the onset of strong localization follows from the equality of the constant classical contribution to the quantum correction, i.e., from the condition $D(\omega = 0) \approx 0$. Doing the integral, we obtain the equivalent condition (for $d = 4$)

$$(4q^2\pi^3)^{1/5}\frac{K_c}{8\tilde{h}} = O(1), \tag{7}$$

which is well satisfied by the observed value $K_c \approx 11.8$ [at which the left-hand side of Eq. (7) equals 1.4].

Beyond perturbation theory [8,19], the diffusion coefficient $D(\omega)$ scales as $D(\omega) = \omega^{\frac{1}{3}} f[(K - K_c)\omega^{-\frac{1}{3\nu}}]$, where $f(x)$ is some scaling function, and $\nu > 0$ is the localization length critical exponent, i.e., $\xi \sim (K_c - K)^{-\nu}$. Noting that $\omega \sim t^{-1}$, we conclude that in the virtual space, the wave-packet expansion saturates at large times when $(K_c - K)t^{\frac{1}{3\nu}} \gg 1$. This implies that in the supermetallic phase, the metal-supermetal crossover occurs at $t_\xi \sim (K_c - K)^{-3\nu}$, i.e., we have arrived at the identification $\alpha = 3\nu$. Our simulations predict that $1.4 \leqslant \nu \leqslant 1.6$, which is consistent with general results for the three-dimensional Anderson transition of the unitary type [20].

The above results for K_c and α corroborate the view that the phase transition observed at $q = 3$ is in the universality class of the Anderson metal-insulator transition. Below the critical value $K = K_c$, the system effectively behaves as a finite system of extension $q\xi^3$ and finite-size quantization of energy levels then is responsible for the supermetallic scaling of response coefficients.

V. ANOMALOUS SUPERMETALLIC BEHAVIOR AT $q = 4$

Numerical experiments further show that for larger values of q $(= 5,6,7,\ldots)$, the QKR behaves in the same way as the $q = 3$ case. This suggests that the unconventional quantum criticality occurs for generic q. This notwithstanding, anomalous behavior is observed for $q = 4$: Regardless of the dimension d, the energy growth exhibits a linear-quadratic

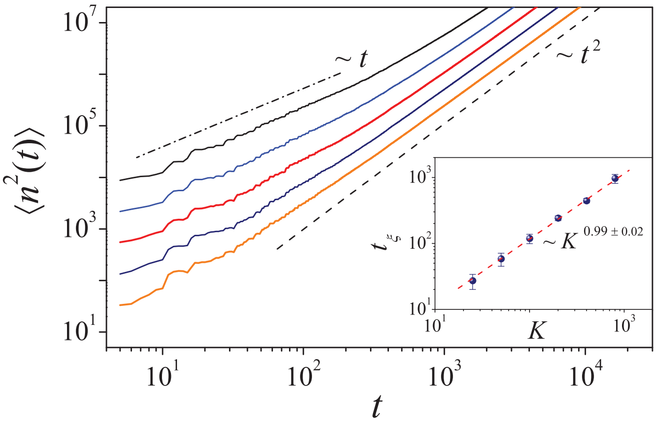

FIG. 7. (Color online) The anomalous energy growth for $q = 4$ with $d = 3$. In the main panel, the solid curves (from bottom to top) are for $K = 25,50,100,200$, and 400, respectively. The inset shows t_ξ as a function of K.

crossover with the crossover time $t_\xi \sim K$. (See Fig. 7 as exemplified by the case of $d = 3$).

To understand why unusual things happen at this q value, notice that in the QKR context, the kinetic-energy operator $\exp(-i\tilde{h}\frac{\hat{n}^2}{2})$ plays the role of a stochastic scattering operator, much like a random real-space potential in conventional Anderson localization. Our analysis thus far presumes that this operator does not exhibit any regular structure throughout the unit cell, $n = 0,\dots,q-1$. However, for $q = 4$, this operator is translationally invariant in 2 and the unit cell, $\{0,1,2,3\}$, splits into two replicated subcells, $\{0,1\}$ and $\{2,3\}$. Most interestingly, this reduction renders the rotor similar to its genuine two-periodic sibling: the only difference is that in the former (latter), the factor $\exp(-i\tilde{h}\frac{n^2}{2})$ takes the value of $-i$ (-1) for odd n. On general grounds, we expect the dynamics to be (partially) regular. Indeed, we find that the level spacing distribution is dramatically different from the $q = 3$ case: strikingly, it is symmetric with respect to $s = 1$ and, only for small s, it follows the Wigner surmise of the CUE type [see Fig. 5(b)].

Moreover, our numerical analysis for $q = 4$ shows that an initial regime of diffusion—a manifestation of stochasticity—is followed by a strong tendency to localize in the auxiliary dimensions already at times $t > K$ parametrically shorter than in the generic case (cf. Fig. 7). While we do not fully understand the origin of this behavior, it appears to be outside the standard Anderson universality class. In addition, it is interesting to notice that at $q = 4$, no localization-delocalization transition is observed. We believe that this is a manifestation of a partial restoration of regular dynamics. Further research is required to understand these phenomena and to explore whether or not there exist any other anomalous q values.

VI. DISCUSSION

In this paper, we have numerically explored the QKR driven by $d-1$ incommensurate frequencies and at resonant values of Planck's constant $\tilde{h} = 4\pi/q$. Compared to the standard rotor, the presence of additional driving frequencies and the fine tuning of Planck's constant provide the option to realize qualitatively different types of quantum criticality. We have seen that depending on the value of q, the system may be exactly solvable (reflecting the regular nature of quantum dynamics) at $q = 1,2$, may be in the Anderson universality class on a circumference q cylinder of dimensionality d ($q = 3,5,6,\dots$), or may be in an anomalously localized regime ($q = 4$). The option to change the universality class of the system by a well-defined change of a single control parameter provides us with a high-quality test bed of our understanding of Anderson-type quantum criticality. It stands to reason that the configurations explored in this paper, $d = 2,3,4$ and $q = 1,2,3,4$, are within the reach of state-of-the-art atom-optics setups [10–12,19,21–24]. In current experiments, the expansion of atomic clouds can be observed over several hundred kicks [10–12,19] and a quantitative comparison to our results should be possible.

ACKNOWLEDGMENTS

Discussions with D. Delande, S. Fishman, J. C. Garreau, and I. Guarneri are gratefully acknowledged. This work is supported by the NSFC (Grants No. 11275159, No. 11335006, and No. 11174174), the Tsinghua University ISRP, and the Sonderforschungsbereich TR12 of the Deutsche Forschungsgemeinschaft.

APPENDIX: EXACT SOLUTION AT $q = 1,2$

For $q = 1,2$, the quantum dynamics (3) is exactly solvable. Staying in the ungauged one-dimensional representation of the system, we find that in the angular momentum (n) representation, the matrix element of $\hat{U}'(s)$ reads

$$\langle n|\hat{U}'(s)|n'\rangle = \begin{cases} J_{n-n'}\left[\frac{K}{\tilde{h}} f_d(s)\right], & q = 1 \\ (-)^n J_{n-n'}\left[\frac{K}{\tilde{h}} f_d(s)\right], & q = 2, \end{cases} \tag{A1}$$

where $J_n(x)$ is the Bessel function. With the help of the identity

$$\sum_{k=-\infty}^{\infty} J_{n\mp k}(x) J_k(x') = J_n(x \pm x'),$$

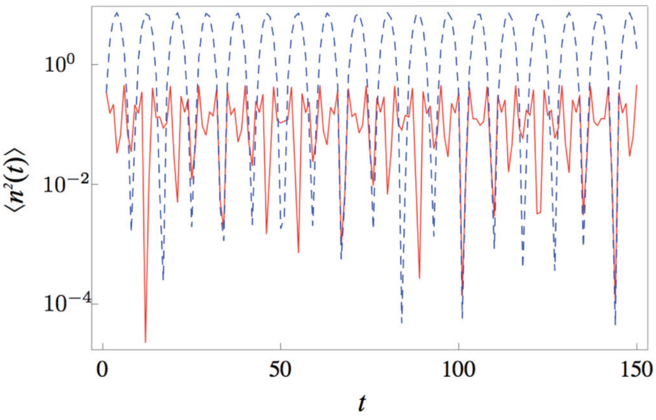

FIG. 8. (Color online) For $d = 2$, the analytic result (A4) shows that $\langle \hat{n}^2(t)\rangle$ [in units of $\frac{1}{2}(K/\tilde{h})^2$] exhibits quasiperiodic oscillations at both $q = 1$ (red solid lines) and $q = 2$ (blue dashed lines). The parameters $(\omega_1,\phi_1) = 2\pi[(\sqrt{5}-1)/2,\sqrt{3}-1]$.

it is straightforward to derive

$$\langle n|\prod_{s=1}^{t}\hat{U}'(s)|m\rangle = \begin{cases} J_{n-m}\left[\frac{K}{\tilde{h}}\sum_{s=1}^{t} f_d(s)\right], & q=1 \\ (-)^{n-m\delta_{1,\mathrm{P}_t}} J_{n-m}\left[\frac{K P_t}{\tilde{h}}\sum_{s=1}^{t}(-)^s f_d(s)\right], & q=2, \end{cases} \tag{A2}$$

from (A1). Using these matrix elements and the identity

$$\sum_{k=-\infty}^{\infty} k^2 J_k^2(x) = \frac{x^2}{2},$$

we obtain Eq. (6).

Next, we apply the above general analysis to the simplest case of $d=2$, with $f_2(t)=\cos(\omega_1 t+\phi_1)$. It is straightforward to verify that

$$\sum_{s=1}^{t} f_2(s) = \begin{cases} \frac{\cos(\omega_1+\phi_1)-\cos\phi_1-\cos[\omega_1(t+1)+\phi_1]+\cos(\omega_1 t+\phi_1)}{2(1-\cos\omega_1)}, & q=1 \\ \frac{-\cos(\omega_1+\phi_1)-\cos\phi_1+(-)^t\{\cos[\omega_1(t+1)+\phi_1]+\cos(\omega_1 t+\phi_1)\}}{2(1+\cos\omega_1)}, & q=2. \end{cases} \tag{A3}$$

Substituting it into Eq. (6) gives

$$\frac{\langle \hat{n}^2(t)\rangle}{\frac{1}{2}(K/\tilde{h})^2} = \begin{cases} \frac{\{\cos(\omega_1+\phi_1)-\cos\phi_1-\cos[\omega_1(t+1)+\phi_1]+\cos(\omega_1 t+\phi_1)\}^2}{4(1-\cos\omega_1)^2}, & q=1 \\ \frac{\left[\cos(\omega_1+\phi_1)+\cos\phi_1-(-)^t\{\cos[\omega_1(t+1)+\phi_1]+\cos(\omega_1 t+\phi_1)\}\right]^2}{4(1+\cos\omega_1)^2}, & q=2. \end{cases} \tag{A4}$$

As shown in Fig. 8, the energy exhibits quasiperiodic oscillations at $d=2$, similar to the $d=3$ case discussed in Sec. III.

[1] G. Casati, B. V. Chirikov, J. Ford, and F. M. Izrailev, in *Stochastic Behavior of Classical and Quantum Hamiltonian Systems*, edited by G. Casati and J. Ford, Lecture Notes in Physics (Springer, New York, 1979), Vol. 93.

[2] F. M. Izrailev, Phys. Rep. **196**, 299 (1990).

[3] B. Chirikov and D. Shepelyansky, Scholarpedia **3**, 3550 (2008).

[4] S. Fishman, Scholarpedia **5**, 9816 (2010).

[5] S. Fishman, D. R. Grempel, and R. E. Prange, Phys. Rev. Lett. **49**, 509 (1982).

[6] D. R. Grempel, R. E. Prange, and S. Fishman, Phys. Rev. A **29**, 1639 (1984).

[7] C. Tian and A. Altland, New J. Phys. **12**, 043043 (2010).

[8] C. Tian, A. Altland, and M. Garst, Phys. Rev. Lett. **107**, 074101 (2011).

[9] F. L. Moore, J. C. Robinson, C. F. Bharucha, B. Sundaram, and M. G. Raizen, Phys. Rev. Lett. **75**, 4598 (1995).

[10] J. Chabé, G. Lemarié, B. Grémaud, D. Delande, P. Szriftgiser, and J. C. Garreau, Phys. Rev. Lett. **101**, 255702 (2008).

[11] G. Lemarié, H. Lignier, D. Delande, P. Szriftgiser, and J. C. Garreau, Phys. Rev. Lett. **105**, 090601 (2010).

[12] M. Lopez, J. F. Clément, P. Szriftgiser, J. C. Garreau, and D. Delande, Phys. Rev. Lett. **108**, 095701 (2012).

[13] S. Wimberger, I. Guarneri, and S. Fishman, Nonlinearity **16**, 1381 (2003).

[14] M. Sadgrove and S. Wimberger, Adv. At. Mol. Opt. Phys. **60**, 315 (2011).

[15] F. M. Izrailev and D. L. Shepelyansky, Teor. Mat. Fiz. **43**, 417 (1980) [Theor. Math. Phys. **43**, 553 (1980)].

[16] I. Dana, E. Eisenberg, and N. Shnerb, Phys. Rev. E **54**, 5948 (1996).

[17] C. Tian and A. Altland (unpublished).

[18] G. Casati, I. Guarneri, and D. L. Shepelyansky, Phys. Rev. Lett. **62**, 345 (1989).

[19] G. Lemarié, J. Chabé, P. Szriftgiser, J. C. Garreau, B. Grémaud, and D. Delande, Phys. Rev. A **80**, 043626 (2009).

[20] K. Slevin and T. Ohtsuki, Phys. Rev. Lett. **78**, 4083 (1997).

[21] W. H. Oskay, D. A. Steck, V. Milner, B. G. Klappauf, and M. G. Raizen, Opt. Commun. **179**, 137 (2000).

[22] M. B. d'Arcy, R. M. Godun, M. K. Oberthaler, D. Cassettari, and G. S. Summy, Phys. Rev. Lett. **87**, 074102 (2001).

[23] C. Ryu, M. F. Andersen, A. Vaziri, M. B. d'Arcy, J. M. Grossman, K. Helmerson, and W. D. Phillips, Phys. Rev. Lett. **96**, 160403 (2006).

[24] J. F. Kanem, S. Maneshi, M. Partlow, M. Spanner, and A. M. Steinberg, Phys. Rev. Lett. **98**, 083004 (2007).